Extreme Mechanics Letters 65 (2023) 102091

Contents lists available at ScienceDirect

Extreme Mechanics Letters

journal homepage: www.elsevier.com/locate/eml

Conformally graded metamaterials for elastic wave guidance

Charles Dorn, Dennis M. Kochmann *

Mechanics & Materials Lab, Department of Mechanical and Process Engineering, ETH Zürich, 8092 Zürich, Switzerland

ARTICLE INFO

Keywords:
Metamaterial
Elasticity
Wave guide
Dispersion relation
Conformal mapping

ABSTRACT

Although metamaterials have been widely used for controlling elastic waves through bandgap engineering, the directed guidance of stress waves in non-periodic structures has remained a challenge. This work demonstrates that spatially graded metamaterials based on conformal mappings present a rich design space for controlling and attenuating wave motion — without the need for bandgaps. Conformal mappings transform an elementary unit cell by scaling and rotation into graded lattices with approximately geometrically similar unit cells. This self-similarity allows for control over the local wave dispersion throughout the metamaterial. As a key mechanism, it is shown that elastic waves cannot propagate through graded unit cells with significant size differences, except at low frequencies. This is exploited to create low-pass elastic wave guides, extending beyond classical bandgap engineering, since bandgaps are not required to achieve wave guiding and attenuation. Experiments confirm the low-pass elastic wave filtering capability of a planar truss metamaterial with conformal grading. Finally, a systematic design of curved metamaterial surfaces is presented, providing a flexible framework for programming low-pass attenuation and wave guiding in three dimensions.

1. Introduction

Lattices appear naturally in atomic crystals, where wave dispersion has been studied for decades [1] and plays a fundamental role in lattice vibrations, electrical and thermal conduction, and the refraction of light. Metamaterials do what nature cannot do: the careful design of lattices, which enables as-designed effective properties. Dispersive phenomena observed at the atomic scales, such as bandgaps (frequency bands where wave propagation is forbidden), can be achieved and exploited by metamaterials on a wide range of length scales. The design of periodic mechanical metamaterials, composed of repeating arrangements of beams, plates, shells, or composite materials, has been well-studied due to their appealing elastic wave attenuation capability arising from bandgaps [2]. However, graded metamaterials with smooth spatial variation of unit cells have remained largely unexplored in the context of elastic wave propagation, despite the immensely increased design space compared to periodic architectures [3].

Motivated by the opportunity to leverage bandgaps for vibration suppression and wave guiding, significant efforts have been made to design and optimize periodic metamaterials with wide bandgaps that span desired frequencies [4–9]. By contrast, spatially graded architectures are less explored but offer a considerably larger design space, since both the unit cell content and its spatial variation can be controlled. For example, bandgaps of different unit cells in a graded metamaterial can combine to produce a wider effective bandgap. This phenomenon, sometimes referred to as rainbow trapping, has been demonstrated for elastic waves in one-dimensional [10–16] and two-dimensional [17–19] metamaterials (where wave attenuation has been demonstrated along a specific direction only). While existing research highlights the promise of graded metamaterials for wave manipulation, systematic methods that explore the vast design space of spatially graded lattices have remained an open challenge.

In this work, we present metamaterials graded by conformal mappings, which we show to be effective for mechanical wave attenuation and wave guiding. Conformal mappings consist of a locally uniform scaling and rotation, ensuring that each unit cell in the graded lattice is approximately scaled and rotated. Hence, all unit cells are approximately geometrically similar. Due to this self-similarity, we show that waves cannot propagate along trajectories that see a significant change in unit cell size, except at low frequencies. A simple yet powerful design principle follows: designing regions with a significant unit cell size difference ensures that waves cannot propagate between these regions. As a result, certain regions can be isolated from high-frequency wave propagation. Additionally, we show that attenuation via spatial grading is achievable in the absence of bandgaps, as long as neighboring dispersion surfaces are non-intersecting.

Our use of conformal mappings for mechanical metamaterials is distinct from their extensive use for optical metamaterials. Transformation

* Corresponding author.
E-mail address: dmk@ethz.ch (D.M. Kochmann).

https://doi.org/10.1016/j.eml.2023.102091
Received 23 June 2023; Received in revised form 23 August 2023; Accepted 10 October 2023
Available online 12 October 2023

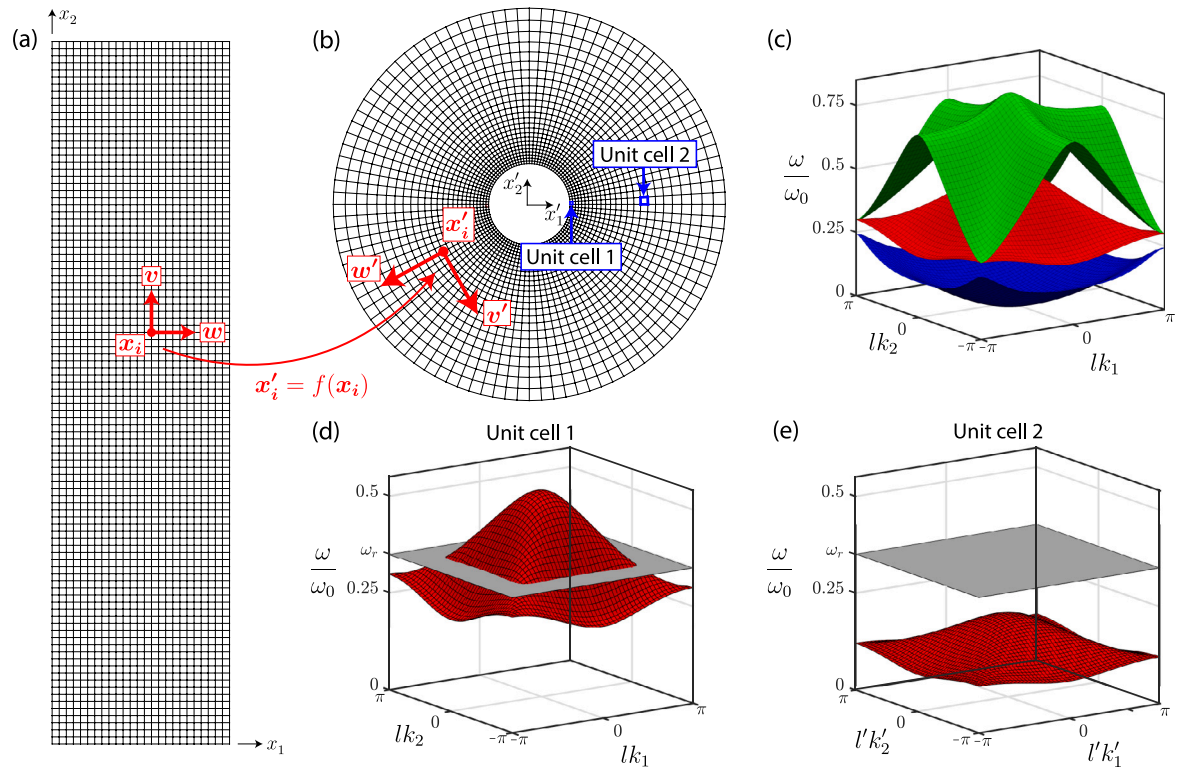

Fig. 1. Planar truss lattice for low-pass attenuation: (a) Reference periodic truss lattice. (b) Graded truss lattice corresponding to a conformal mapping of the reference lattice. (c) Dispersion relations of the reference lattice with unit cell side length l and $\omega_0 = l^{-1}\sqrt{E/\rho}$. (d) Second dispersion surface of unit cell 1, and (e) of unit cell 2 highlighted in (b), with the ω_r level set highlighted.

optics often relies on conformal mappings to achieve practical effective material parameters [20–23] (similarly for transformation acoustics [24–27]). However, transformation optics and acoustics typically apply in the non-dispersive setting [28], requiring sub-wavelength unit cells. Furthermore, they do not directly generalize to elastodynamics due to a lack of form invariance [29].

In the elastodynamic setting, conformal maps have primarily been utilized in the low-frequency and long-wavelength (with respect to a unit cell) regime by relying on effective continuum properties [30–34], which apply only in the homogenization limit [35] , thus missing out on the rich dispersive behavior arising in the short-wavelength regime that is key to mechanical metamaterials. In contrast to previous work, we utilize conformal mappings to control waves at high frequencies and short wavelengths, beyond the homogenization limit, by utilizing the full dispersion relations. To this end, with inspiration from the discrete geometry literature [36–38], we design planar and curved conformally graded metamaterial surfaces. While conformal mappings represent only a fraction of the spatial grading design space, we show that their wave dynamics can be engineered using a simple but general design procedure.

The resulting spatially graded metamaterials appeal to a wide range of applications across scales. Their broad effective bandgaps are practical for vibration suppression, e.g., to shield infrastructure from seismic waves [39]. Grading is also appealing for energy harvesting by trapping or focusing waves [40,41]. Additionally, frequency-selective sensing and signal processing capabilities are enabled by spatial grading [42,43]. The conformal architectures presented in this work enhance the applicability of graded metamaterials by offering low-pass attenuation capabilities without relying on bandgaps. Furthermore, we propose a systematic design method for curved metamaterial surfaces, which offers a flexible tool for programmable wave guidance and attenuation.

2. Conformally graded metamaterials

We design spatially graded lattices through a mapping $f : \mathcal{M} \mapsto \mathbb{R}^3$, which transforms a planar, *periodic* reference lattice $\mathcal{M} \subset \mathbb{R}^2$ into a *graded* lattice $\mathcal{M}' \subset \mathbb{R}^3$. Surface $\mathcal{M}'$ can be flat or curved (both cases will be illustrated). We denote points in the reference lattice by $\boldsymbol{x} \in \mathcal{M}$ and their mapped position in the graded lattice by $\boldsymbol{x}' = f(\boldsymbol{x}) \in \mathcal{M}'$.

The differential $\mathrm{d}f = \frac{\mathrm{d}\boldsymbol{x}'}{\mathrm{d}\boldsymbol{x}}$ of the mapping defines how a vector $\boldsymbol{v} \in \mathbb{R}^2$ maps to the vector $\boldsymbol{v}' = \mathrm{d}f(\boldsymbol{v}) \in \mathbb{R}^3$ (i.e., it characterizes how vectors tangent to the reference lattice map onto the corresponding vectors tangent to the graded lattice). The mapping is *conformal*, if $\mathrm{d}f(\boldsymbol{v}) \cdot \mathrm{d}f(\boldsymbol{w}) = J^2 \boldsymbol{v} \cdot \boldsymbol{w}$, where $J > 0$ is the *conformal scaling factor*.

Conformal mappings are chosen specifically, because they consist solely of a local uniform scaling (since for any vector $\boldsymbol{v}$ we have $|\mathrm{d}f(\boldsymbol{v})| = J|\boldsymbol{v}|$) and a rotation (since the angle between vectors is unchanged by the mapping) of the unit cells. Fig. 1ab illustrates a conformal mapping in the case where $\mathcal{M}'$ is planar. Here, the vectors $\boldsymbol{v}$ and $\boldsymbol{w}$, which are attached to the reference lattice at point $\boldsymbol{x}_i$, are uniformly scaled and rotated by the mapping to vectors $\boldsymbol{v}'$ and $\boldsymbol{w}'$, while the angle between them is preserved. For a more extensive treatment of conformal mappings, see [44,45].

We assume that in the transformed lattice the unit cells vary slowly in space, so that $\mathrm{d}f$ can be taken as constant throughout any given unit cell. Under this assumption, each unit cell undergoes only uniform scaling by a factor J and a rotation. This assumption allows the graded lattice to be modeled as *locally periodic*, so that wave propagation is governed by the *local dispersion relations* [3]. That is, the local dispersion relations at a given unit cell on the graded lattice are calculated assuming periodicity of that unit cell, which is a valid approximation for slow spatial gradings.

Conformal grading yields a special case of local periodicity since, under the above assumptions, all unit cells are geometrically similar to the unit cell of the reference lattice. Consider a reference unit cell with dispersion relations $\omega(\boldsymbol{k})$, relating the wave vector $\boldsymbol{k} \in \mathbb{R}^2$ to the

frequency ω of an elastic plane wave. A unit cell in the transformed lattice has local dispersion relations $\omega'(\boldsymbol{k}')$. Since this unit cell is a scaled and rotated copy of the reference unit cell, its dispersion relations take the form

$$\omega'(\boldsymbol{k}') = \boldsymbol{J}^{-1}\omega(\boldsymbol{k}), \tag{1}$$

where $\boldsymbol{k}'$ is the wave vector in the transformed coordinates (a derivation is provided in Section 1 of the Supplementary Material, which holds generally for linear elastic waves). For the example mapping in Fig. 1, the dispersion relations of the reference lattice (Fig. 1c) are hence simply re-scaled to determine the local dispersion relations of any unit cell in the graded lattice, including unit cells 1 (Fig. 1d) and 2 (Fig. 1e).

To understand how to exploit this inverse frequency scaling relation, we view wave propagation from the perspective of ray theory. Ray theory has long been used to model wave propagation in many fields, ranging from optics [46] to seismology [47], where it provides approximate solutions to a wave equation along characteristic ray trajectories. We recently extended it to graded elastic metamaterials [3], under the assumption that wavelengths are significantly smaller than the length scale associated with the spatial grading of the unit cells. Ray theory is valid in the context of high frequencies and short wavelengths, i.e., when unit cells change slowly in space relative to the wavelength, which is the context considered here.

We rely on two key properties of rays to reveal the special properties of conformally graded lattices in the linear elastic regime:

(i) A ray propagates at a fixed frequency.
(ii) A ray is associated with a particular dispersion surface (i.e., a particular mode). It cannot switch between modes as long as the unit cells vary slowly in space and no frequency degeneracies are encountered.

Property (i) holds as long as the local dispersion relations are time-invariant [48], which is generally the case for elastic media. Property (ii) is a re-statement of the adiabatic theorem, which is well-known in quantum mechanics [49] but also applies to elastodynamics [50].

Combining Properties (i) and (ii) with the dispersion scaling law of Eq. (1) admits a general observation about elastic wave propagation in conformally graded lattices: *high-frequency waves cannot propagate along trajectories that see significant changes in unit cell size*. This becomes evident as follows. By Eq. (1), local dispersion surfaces everywhere are a scaled copy of the reference dispersion surfaces. By Properties (i) and (ii), a ray is confined to a level set of a given mode's dispersion surface corresponding to the ray's fixed frequency ω_r (e.g., in Fig. 1d, a ray's wave vector must lie on the intersection of the dispersion surface and the ray's fixed frequency ω_r). If that dispersion surface has a nonzero minimum frequency, it is always possible to scale that surface up or down such that it no longer intersects ω_r (e.g., in Fig. 1e there is no intersection between ω_r and the scaled dispersion surface). This scaling argument, however, does not apply at low frequencies of dispersion surfaces emerging from $\omega = 0$ (the so-called acoustic modes).

By this scaling argument, attenuation via spatial grading is achievable when adjacent dispersion surfaces are non-intersecting. When adjacent dispersion surfaces intersect, Property (ii) (the adiabatic theorem) does not hold and mode conversion may occur. We rely on the argument that, when a propagating wave becomes forbidden, it cannot convert to another (non-forbidden) mode, which motivates the requirement of non-intersecting dispersion surfaces. A bandgap ensures that adjacent dispersion surfaces are non-intersecting, but it is also possible to have non-intersecting dispersion surfaces that are not separated by a bandgap. Thus, attenuation is also possible in the absence of a bandgap if adjacent dispersion surfaces are non-intersecting (e.g., the lowest two surfaces of Fig. 1c), as we show in the following examples.

3. A planar truss lattice for low-pass attenuation

An instructive example that demonstrates the use of a conformal grading for wave attenuation is a planar truss lattice that acts as a low-pass filter of elastic waves. Consider the conformal mapping

$$z' = e^z, \tag{2}$$

where $z' = x_1' + \mathrm{i}x_2'$, $z = x_1 + \mathrm{i}x_2$ in 2D, and $\mathrm{i} = \sqrt{-1}$. Fig. 1 illustrates this mapping, which conformally transforms the reference lattice with square unit cells (Fig. 1a) to a radial lattice (Fig. 1b). In the transformed lattice, the outermost unit cells are $J_\mathrm{o} = 3.51$ times larger than the innermost ones, which have $J_\mathrm{i} = 1$, where J_o and J_i are scaling factors with respect to the reference lattice.

Each unit cell consists of slender linear elastic beams along its four edges. Dispersion relations for the reference unit cell are computed numerically using a beam finite element model of a unit cell (Supplementary Material, Section 2). The first three dispersion surfaces corresponding to out-of-plane modes are plotted in Fig. 1c over the first Brillouin zone, with frequencies normalized by $\omega_0 = l^{-1}\sqrt{E/\rho}$, where l is the edge length of the reference unit cell, and E and ρ are Young's modulus and the mass density of the beams' base material. The lowest modes of truss lattices are decoupled into in- and out-of-plane modes [51]; by considering out-of-plane excitation, only the out-of-plane modes must be considered.

This conformally graded truss lattice acts as a low-pass filter for waves applied to the center of the lattice; waves above a cutoff frequency cannot propagate from the inner to the outer radius. To illustrate this, consider a mode 2 ray that starts in unit cell 1 of Fig. 1 and propagates radially outward at the excitation frequency ω_r. In unit cell 1, the wave vector of this ray must lie on the intersection of the mode 2 (red) dispersion surface and the ω_r level-set (gray), as depicted in Fig. 1d. Moving to unit cell 2, which is 2.73 times larger than unit cell 1, its dispersion surface is obtained by scaling the frequency of unit cell 1's dispersion surface by a factor of $1/2.73$. At unit cell 2, there is no intersection between the mode 2's dispersion surface and the ω_r level set (Fig. 1e). Therefore, a mode 2 ray starting at unit cell 1 with frequency ω_r is forbidden in unit cell 2. Supplementary Video S1 visualizes the dispersion surface as the unit cell is re-scaled, highlighting the critical scaling factor where propagation at frequency ω_r becomes forbidden.

By applying this scaling argument more generally, rays of all frequencies (except those approaching $\omega = 0$ of mode 1) become forbidden for a sufficiently large scaling factor, corresponding to when the dispersion surface is scaled to no longer intersect the frequency of the ray. Thus, rays starting at unit cell 1 will reach some maximum radius, beyond which propagation is forbidden. Based on this dispersion scaling argument, the critical radius is computed across a range of frequencies and plotted in Fig. 2e. Regions where propagation is allowed are highlighted in red, and regions where a wave starting at the inner radius is forbidden are white. Details of the scaling analysis are given in Section 2.3 of the Supplementary Material, where care is taken to account for mode conversion due to frequency degeneracies where dispersion surfaces intersect.

We experimentally demonstrate the attenuation capability of this geometry, using the prototype in Fig. 2a, which is made of aluminum and has a tapered thickness to ensure that all unit cells are geometrically similar (see the close-up view in Fig. 2b). Broadband excitation was applied to the center by a piezoelectric (PZT) transducer in the out-of-plane direction. The out-of-plane displacement was measured with a scanning laser Doppler vibrometer, as illustrated in Fig. 2c. Details of the fabrication and experiment are presented in Section 2.2 of the Supplementary Material.

The experimental results in Fig. 2d show the amplitude of the frequency response function (FRF) [52], denoted $H(r', f)$, between the displacement at radial coordinate r' and the inner radius. This provides a measure of attenuation as a wave travels outward from the inner

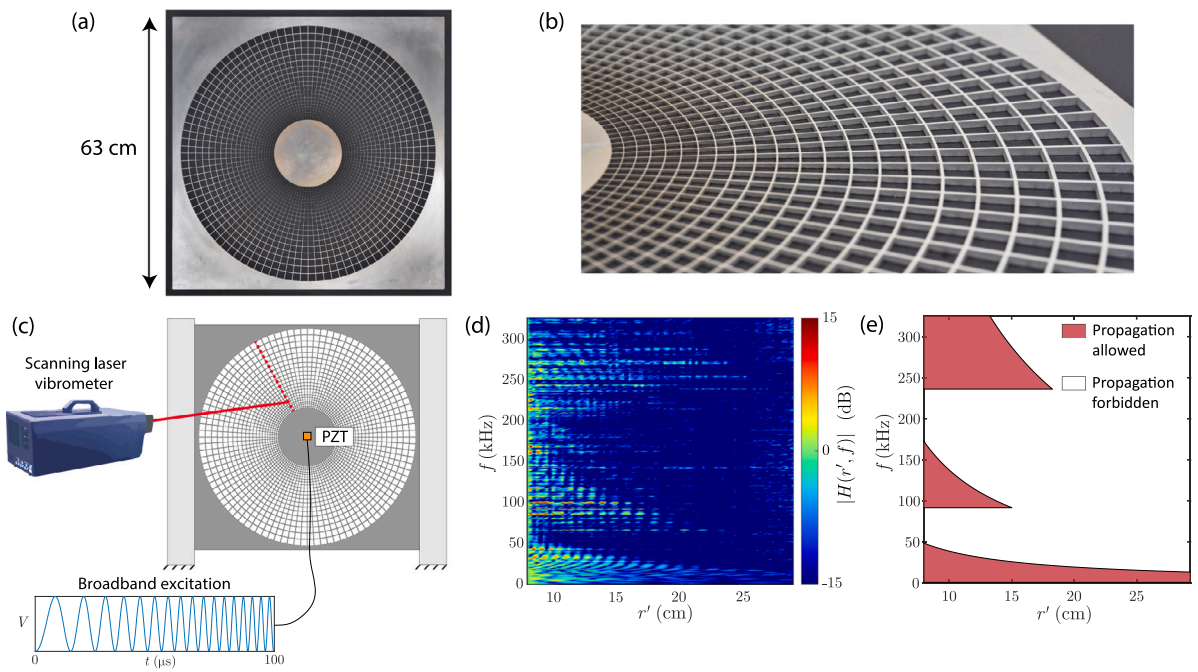

Fig. 2. Experimental confirmation of the low-pass attenuation in a conformally graded truss: truss lattice prototype from the top view (a) and a close-up view (b). (c) Experimental setup: a piezoelectric transducer excites the lattice, whose response is measured by a scanning laser Doppler vibrometer along radial lines. (d) Measured FRF amplitude along a radial line. (e) Predicted regions of allowed and forbidden propagation based on dispersion relation scaling.

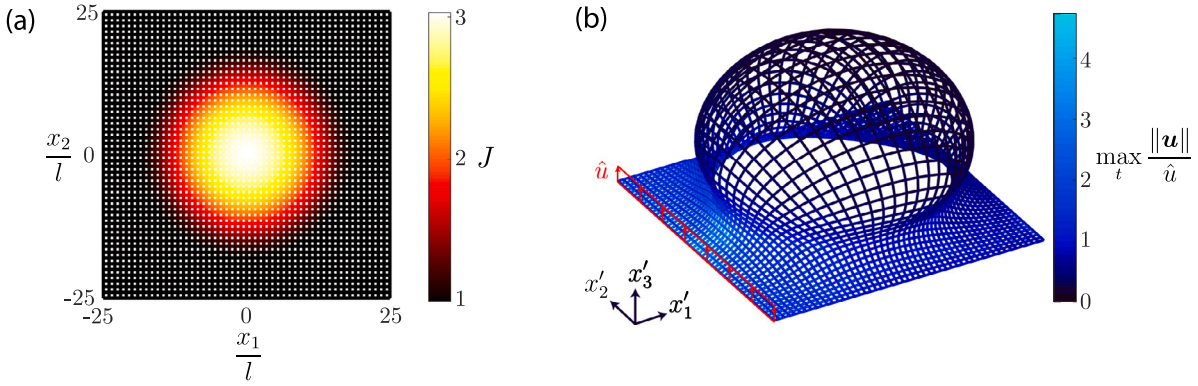

Fig. 3. Conformal bump example. (a) Target scaling factor distribution plotted on the reference lattice. (b) Optimal conformal truss lattice realizing the prescribed scaling. Color indicates the maximum amplitude during a finite element simulation with broadband excitation applied on the lower left edge (highlighted in red) with amplitude $\hat{u}$. (For interpretation of the references to color in this figure legend, the reader is referred to the web version of this article.)

radius by interpreting the displacement signal at the inner radius as the input to the truss. Regions with high FRF amplitude in Fig. 2d agree closely with allowable propagation regions in Fig. 2e, whereas regions of low values correspond to the predicted regions of forbidden propagation. Based on the dispersion relation scaling analysis, the predicted low-pass cutoff frequency is 14.7 kHz; higher frequencies are predicted to be attenuated before reaching the outer radius of the lattice. This prediction agrees with the experimental low-pass cutoff frequency, which is observed to be about 16 kHz.

4. Curved metamaterial surfaces

In addition to the above plane-to-plane case, the same physical principles apply to conformal mappings that transform a planar surface into a curved surface, for which we propose a systematic design framework for curved conformal lattice surfaces. Based on the guiding principle that waves do not propagate between unit cells with a significant scaling difference, our objective is to control the conformal scaling factor distribution in the lattice in order to either isolate a region from incident high-frequency waves or to confine waves in a specified region. The advantage of curved surfaces is that curvature offers a richer design space than planar lattices, allowing for elaborate scaling factor distributions to be realized as follows. Based on a desired unit cell scaling distribution, a target conformal scaling factor distribution $J(\boldsymbol{x})$ is first prescribed on a planar reference lattice. Next, an optimization problem identifies a transformed three-dimensional (3D) lattice that best realizes the prescribed scaling factor distribution.

We approach this problem from the perspective of discrete differential geometry, which naturally follows from the discrete nature of the lattice. In the discrete setting, the target scaling distribution is achieved by re-scaling the edges from the reference length l to a target length $\tilde{l}$. The target edge lengths are carefully chosen to satisfy discrete conformal equivalence [36], as detailed in the Supplemental Material, Section 3.1.

The problem of computing a 3D embedding (i.e., vertex coordinates $\boldsymbol{x}'$) of a discrete surface given its discrete metric (i.e., edge lengths $\tilde{l}$) has been addressed in the discrete differential geometry literature [53–56]. Inspired by these approaches, to compute the transformed vertex

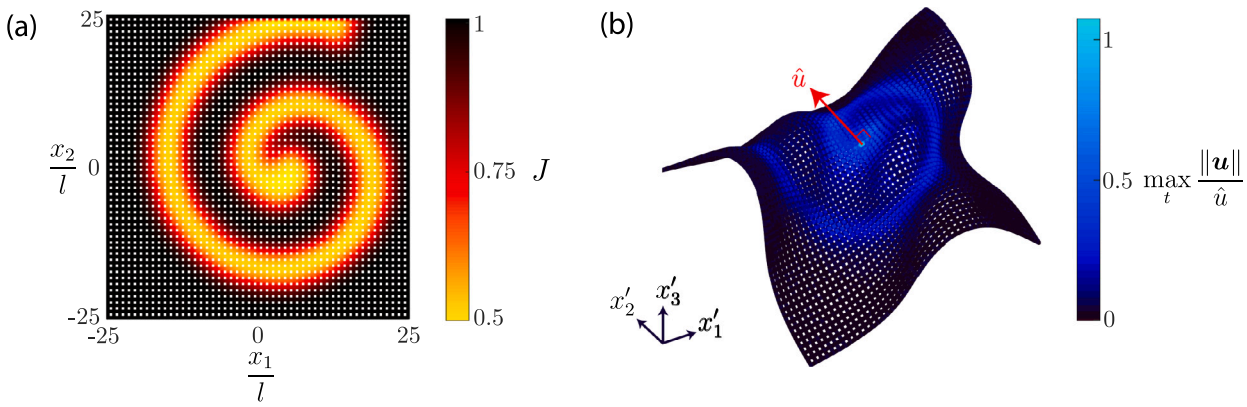

Fig. 4. Conformal spiral example. (a) Target conformal scaling factor distribution plotted on the reference lattice. (b) Optimal conformal truss lattice realizing the prescribed scaling. Color indicates the maximum amplitude during a finite element simulation with a harmonic point excitation of displacement amplitude $\hat{u}$ perpendicular to the surface (along the red arrow). (For interpretation of the references to color in this figure legend, the reader is referred to the web version of this article.)

coordinates $\boldsymbol{x}'$ we pose the unconstrained minimization

$$\min_{\boldsymbol{x}'} E(\boldsymbol{x}'), \tag{3}$$

where

$$E(\boldsymbol{x}') = \sum_m k\left(l_m(\boldsymbol{x}') - \tilde{l}_m\right)^2 + \sum_n \kappa\, \theta_n(\boldsymbol{x}')^2. \tag{4}$$

Here, m indexes all edges and n indexes the interior edges, which are not on the boundary. This optimization can be interpreted as an energy minimization problem by imagining that an extensional spring is placed on each edge, with stiffness k and rest length $\tilde{l}$. In practice, a regularization term is required to achieve smooth solutions, otherwise the optimal surfaces will be 'crumpled' [56]. To this end, the second term in Eq. (4) effectively places a torsional spring on all interior edges with torsional stiffness κ and zero rest angle (the latter corresponds to a flat configuration when the faces connected to the edge are co-planar). This term penalizes crumpled configurations in favor of smoother solutions. Smooth unit cell variations are further essential to avoid sharp kinks, which may invalidate Property (ii) by leading to mode conversion or in-plane and out-of-plane mode coupling.

Fig. 3 presents the example of a *conformal bump*. The reference lattice is planar with uniform square unit cells comprised of beams along each edge. The scaling factor is defined according to a radial bump function and is plotted in Fig. 3a on the reference lattice. It leads to large unit cells in the center with a maximum scaling factor of $J = 3.0$, surrounded by smaller unit cells of $J = 1$ outside of the bump; the optimal 3D geometry is plotted in Fig. 3b. (Constraints were added to fix the four boundaries of the lattice; for implementation details, see Section 3 of the Supplementary Material.) The bump in the center of the transformed lattice, which contains large unit cells, is isolated from high-frequency waves initiated on the boundaries of the lattice, whose smaller unit cells support those frequencies. To demonstrate this effect, a transient finite element simulation was performed. In the simulation, broadband displacement excitation was applied on the lower left (red) edge in the x_3'-direction with magnitude $\hat{u}$. Beam elements were used to model the lattice; see the Supplementary Material, Section 3.4 for details. The suppression of waves in the bump region is evident from the color map of Fig. 3b, which shows the maximum displacement magnitude at each point over the duration of the simulation (see also Supplementary Video S2). Importantly, this mechanism is not restricted to a narrow range of frequencies (as is often the case when leveraging bandgaps to manipulate waves). Instead *all* frequencies above the critical frequency (which is controlled by the unit cell scaling factor distribution) are attenuated in the bump region. This effectively extends the benefits of rainbow trapping to, in principle, arbitrarily defined regions. This type of architecture is appealing for vibration isolation applications. For example, sensitive equipment could be mounted to the bump for shielding from high-frequency vibrations. To potentially achieve full attenuation across all frequencies, one could consider metamaterials connected to a foundation, which can exhibit bandgaps starting at zero frequency [57], combined with conformal grading.

Beyond merely attenuating waves, conformal grading also provides a means of designing wave guides. A second example of a *conformal spiral* is presented to demonstrate wave guiding. In this example, a region of small unit cell scaling in the shape of an Archimedean spiral is prescribed, which is plotted on the reference lattice in Fig. 4a. In the spiral region, the smallest scaling factor is $J = 0.47$, while a factor of $J = 1$ is prescribed outside of the spiral region. The optimal lattice surface is plotted in Fig. 4b, which takes the form of a wavy surface to accommodate the smaller unit cells along the spiral.

In this example, the path of small unit cells along the spiral is capable of confining waves. We demonstrate this with a transient finite element simulation, where a harmonic displacement point excitation of magnitude $\hat{u}$ is applied at the center of the spiral in the direction locally normal to the surface at that point. The frequency of the excitation is chosen to be near the top of the lowest dispersion surface, such that only a small increase in unit cell size forbids propagation. The resulting wave emanating from the point source follows the path of small unit cells and is thus guided along the spiral. The coloring of Fig. 4b shows the maximum displacement magnitude throughout the lattice during the simulation (see also Supplementary Video S3). This example demonstrates that the spatially graded lattice can be leveraged to effectively steer waves by designing regions of forbidden propagation.

While both examples confirm that waves are attenuated in regions with a large unit cell scaling factor compared to the excitation location, perfect attenuation is not achieved, as may be expected for a number of reasons. The assumption of local periodicity is an approximation. Validity of the local periodicity assumption is difficult to quantify in the elastodynamic setting because the neglected terms of the underlying asymptotic analysis cannot be easily evaluated [3] (in contrast to, e.g., one-dimensional rainbow trapping in optical systems, where the adiabatic parameter provides a simple validity assessment [58]).

Additionally, it is assumed that the 'locally flat' dispersion relations are valid for curved truss lattice surfaces. Specifically, we compute the local dispersion relations based on a flat lattice and assume that they are valid in the local neighborhood of a unit cell on a curved surface. Thus, the role of curvature is primarily to realize unit cell scaling distributions that are not possible with flat surfaces. Through the assumption of locally flat dispersion relations, curvature does not directly affect the local wave dispersion. Of course, for sufficiently aggressive curvature, this assumption would break down. However, for the examples presented, the finite element simulations display the

expected behavior, indicating that the locally flat dispersion relations capture the dominant physics.

Finally, the unit cells are not exactly geometrically similar in these two examples. Nevertheless, our assumptions are sufficiently valid to produce the desired wave confinement and attenuation behavior.

5. Conclusion

We have shown that conformally graded metamaterials effectively attenuate mechanical waves above a controllable cut-off frequency and hence can be designed to behave as effective waveguides — without requiring bandgaps. While metamaterials with broadband attenuation capability have been pursued by a growing body of research, conformally graded architectures go beyond broadband to achieve low-pass attenuation. Furthermore, our dispersion scaling analysis is more general than tracking how bandgaps shift with spatial unit cell variations, which is typically done to study attenuation in graded architectures [17–19]. Specifically, a bandgap between two dispersion surfaces is not required to achieve attenuation, but only the less strict requirement that there is no intersection between neighboring dispersion surfaces. For example, there is no bandgap between the lowest two dispersion surfaces of Fig. 1c; yet, since there is no intersection between them, attenuation via spatial grading is achieved.

While an experimental demonstration confirms the low-pass attenuation capability of a planar lattice, curved lattice surfaces offer a wide design space for conformal grading, whose systematic inverse design shows promise for vibration isolation applications across length scales. This work represents only a small step into the vast and largely unexplored design space of graded and curved metamaterial surfaces. The effectiveness of conformal grading suggests that more general types of grading are promising for linear elastic wave manipulation.

Declaration of competing interest

The authors declare that they have no known competing financial interests or personal relationships that could have appeared to influence the work reported in this paper.

Data availability

Data will be made available on request.

Acknowledgments

This work was supported by an ETH Zürich Postdoctoral Fellowship, Switzerland. The authors thank Vignesh Kannan for assistance with the experimental setup and Bastian Telgen for assistance with dispersion relation computations.

Appendix A. Supplementary data

Supplementary material related to this article can be found online at https://doi.org/10.1016/j.eml.2023.102091.

References

[1] Leon Brillouin, Wave Propagation in Periodic Structures: Electric Filters and Crystal Lattices, Vol. 2, Dover publications, 1953.
[2] Mahmoud I. Hussein, Michael J. Leamy, Massimo Ruzzene, Dynamics of phononic materials and structures: Historical origins, recent progress, and future outlook, Appl. Mech. Rev. 66 (4) (2014).
[3] Charles Dorn, Dennis M. Kochmann, Ray theory for elastic wave propagation in graded metamaterials, J. Mech. Phys. Solids 168 (2022).
[4] Ole Sigmund, Jakob Søndergaard Jensen, Systematic design of phononic band–gap materials and structures by topology optimization, Phil. Trans. R. Soc. A 361 (1806) (2003) 1001–1019.
[5] Søren Halkjær, Ole Sigmund, Jakob S. Jensen, Maximizing band gaps in plate structures, Struct. Multidiscip. Optim. 32 (4) (2006) 263–275.
[6] Sandro L. Vatanabe, Glaucio H. Paulino, Emílio C.N. Silva, Maximizing phononic band gaps in piezocomposite materials by means of topology optimization, J. Acoust. Soc. Am. 136 (2) (2014) 494–501.
[7] Osama R. Bilal, Mahmoud I. Hussein, Ultrawide phononic band gap for combined in-plane and out-of-plane waves, Phys. Rev. E 84 (6) (2011) 065701.
[8] Jakob S. Jensen, Niels L. Pedersen, On maximal eigenfrequency separation in two-material structures: the 1D and 2D scalar cases, J. Sound Vib. 289 (4–5) (2006) 967–986.
[9] Hao-Wen Dong, Xiao-Xing Su, Yue-Sheng Wang, Chuanzeng Zhang, Topological optimization of two-dimensional phononic crystals based on the finite element method and genetic algorithm, Struct. Multidiscip. Optim. 50 (4) (2014) 593–604.
[10] G.J. Chaplain, Daniel Pajer, Jacopo M. De Ponti, Richard V. Craster, Delineating rainbow reflection and trapping with applications for energy harvesting, New J. Phys. 22 (6) (2020) 063024.
[11] G.J. Chaplain, Jacopo M. De Ponti, Giulia Aguzzi, Andrea Colombi, Richard V. Craster, Topological rainbow trapping for elastic energy harvesting in graded su-schrieffer-heeger systems, Phys. Rev. A 14 (5) (2020) 054035.
[12] Jacopo M. De Ponti, Andrea Colombi, Raffaele Ardito, Francesco Braghin, Alberto Corigliano, Richard V. Craster, Graded elastic metasurface for enhanced energy harvesting, New J. Phys. 22 (1) (2020) 013013.
[13] Mustafa Alshaqaq, Alper Erturk, Graded multifunctional piezoelectric metastructures for wideband vibration attenuation and energy harvesting, Smart Mater. Struct. 30 (1) (2020) 015029.
[14] Mustafa Alshaqaq, Christopher Sugino, Alper Erturk, Programmable rainbow trapping and band-gap enhancement via spatial group-velocity tailoring in elastic metamaterials, Phys. Rev. A 17 (2) (2022) L021003.
[15] Bao Zhao, Henrik R. Thomsen, Jacopo M. De Ponti, Emanuele Riva, Bart Van Damme, Andrea Bergamini, Eleni Chatzi, Andrea Colombi, A graded metamaterial for broadband and high-capability piezoelectric energy harvesting, Energy Convers. Manage. 269 (2022) 116056.
[16] Luca Rosafalco, Jacopo Maria De Ponti, Luca Iorio, Raffaele Ardito, Alberto Corigliano, Optimised graded metamaterials for mechanical energy confinement and amplification via reinforcement learning, Eur. J. Mech. A Solids (2023) 104947.
[17] Giuseppe Trainiti, Julian J. Rimoli, Massimo Ruzzene, Wave propagation in undulated structural lattices, Int. J. Solids Struct. 97 (2016) 431–444.
[18] Giuseppe Trainiti, Julian J. Rimoli, Massimo Ruzzene, Optical evaluation of the wave filtering properties of graded undulated lattices, J. Appl. Phys. 123 (9) (2018) 091706.
[19] Giulia Aguzzi, Constantinos Kanellopoulos, Richard Wiltshaw, Richard V. Craster, Eleni N. Chatzi, Andrea Colombi, Octet lattice-based plate for elastic wave control, Sci. Rep. 12 (1) (2022) 1–14.
[20] Ulf Leonhardt, Optical conformal mapping, Science 312 (5781) (2006) 1777–1780.
[21] Borislav Vasić, Goran Isić, Radoš Gajić, Kurt Hingerl, Controlling electromagnetic fields with graded photonic crystals in metamaterial regime, Opt. Express 18 (19) (2010) 20321–20333.
[22] Kan Yao, Xunya Jiang, Designing feasible optical devices via conformal mapping, J. Opt. Soc. Amer. B 28 (5) (2011) 1037–1042.
[23] Lin Xu, Huanyang Chen, Conformal transformation optics, Nat. Photonics 9 (1) (2015) 15–23.
[24] Hui Yuan Dong, Qiang Cheng, Gang Yong Song, Wen Xuan Tang, Jin Wang, Tie Jun Cui, Realization of broadband acoustic metamaterial lens with quasi-conformal mapping, Appl. Phys. Express 10 (8) (2017) 087202.
[25] Zhaoyong Sun, Xuecong Sun, Han Jia, Yafeng Bi, Jun Yang, Quasi-isotropic underwater acoustic carpet cloak based on latticed pentamode metafluid, Appl. Phys. Lett. 114 (9) (2019) 094101.
[26] Erqian Dong, Yangyang Zhou, Yu Zhang, Huanyang Chen, Bioinspired conformal transformation acoustics, Phys. Rev. A 13 (2) (2020) 024002.
[27] Run Yu, Xiaoniu Li, Kangyu Wang, Chunyao Lu, Chunling Zhu, Dawei Wu, Active control of sound waves via three-dimensional quasi-conformal mapping, Appl. Phys. Express 13 (2) (2020) 024003.
[28] Martin McCall, John B. Pendry, Vincenzo Galdi, Yun Lai, S.A.R. Horsley, Jensen Li, Jian Zhu, Rhiannon C. Mitchell-Thomas, Oscar Quevedo-Teruel, Philippe Tassin, et al., Roadmap on transformation optics, J. Opt. 20 (6) (2018) 063001.
[29] Graeme W. Milton, Marc Briane, John R. Willis, On cloaking for elasticity and physical equations with a transformation invariant form, New J. Phys. 8 (10) (2006) 248.
[30] Zheng Chang, Gengkai Hu, Elastic wave omnidirectional absorbers designed by transformation method, Appl. Phys. Lett. 101 (5) (2012) 054102.
[31] Yangyang Chen, Jin Hu, Guoliang Huang, A design of active elastic metamaterials for control of flexural waves using the transformation method, J. Intell. Mater. Syst. Struct. 27 (10) (2016) 1337–1347.
[32] Hexuan Gao, Zhihai Xiang, Manipulating elastic waves with conventional isotropic materials, Phys. Rev. A 11 (6) (2019) 064040.
[33] Hussein Nassar, Y.Y. Chen, G.L. Huang, Isotropic polar solids for conformal transformation elasticity and cloaking, J. Mech. Phys. Solids 129 (2019) 229–243.
[34] Hussein Nassar, Y.Y. Chen, G.L. Huang, Polar metamaterials: a new outlook on resonance for cloaking applications, Phys. Rev. Lett. 124 (8) (2020) 084301.

[35] Stefano Gonella, Massimo Ruzzene, Homogenization and equivalent in-plane properties of two-dimensional periodic lattices, Int. J. Solids Struct. 45 (10) (2008) 2897–2915.
[36] Boris Springborn, Peter Schröder, Ulrich Pinkall, Conformal equivalence of triangle meshes, in: ACM SIGGRAPH 2008 Papers, 2008, pp. 1–11.
[37] Keenan Crane, Ulrich Pinkall, Peter Schröder, Spin transformations of discrete surfaces, in: ACM SIGGRAPH 2011 Papers, 2011, pp. 1–10.
[38] Keenan Crane, Conformal geometry of simplicial surfaces, in: Proceedings of Symposia in Applied Mathematics, American Mathematical Society, 2020.
[39] Andrea Colombi, Daniel Colquitt, Philippe Roux, Sebastien Guenneau, Richard V. Craster, A seismic metamaterial: The resonant metawedge, Sci. Rep. 6 (1) (2016) 27717.
[40] Serife Tol, Fahrettin Levent Degertekin, Alper Erturk, Phononic crystal Luneburg lens for omnidirectional elastic wave focusing and energy harvesting, Appl. Phys. Lett. 111 (1) (2017) 013503.
[41] Jacopo Maria De Ponti, et al., Graded Elastic Metamaterials for Energy Harvesting, Springer, 2021.
[42] Liuxian Zhao, Shengxi Zhou, Compact acoustic rainbow trapping in a bioinspired spiral array of graded locally resonant metamaterials, Sensors 19 (4) (2019) 788.
[43] Tinggui Chen, Wenting Li, Dejie Yu, A tunable gradient acoustic metamaterial for acoustic sensing, Extreme Mech. Lett. 49 (2021) 101481.
[44] Zeev Nehari, Conformal Mapping, Courier Corporation, 2012.
[45] Xianfeng David Gu, Shing-Tung Yau, Computational Conformal Geometry, Vol. 1, International Press Somerville, MA, 2008.
[46] Max Born, Emil Wolf, Principles of Optics: Electromagnetic Theory of Propagation, Interference and Diffraction of Light, Elsevier, 2013.
[47] Vlastislav Cervenỳ, Seismic Ray Theory, Vol. 110, Cambridge University Press Cambridge, 2001.
[48] Kip S. Thorne, Roger D. Blandford, Modern Classical Physics: Optics, Fluids, Plasmas, Elasticity, Relativity, and Statistical Physics, Princeton University Press, 2017.
[49] Jun John Sakurai, Eugene D. Commins, Modern Quantum Mechanics, revised ed., American Association of Physics Teachers, 1995.
[50] H. Nassar, H. Chen, A.N. Norris, G.L. Huang, Quantization of band tilting in modulated phononic crystals, Phys. Rev. B 97 (1) (2018) 014305.
[51] Alex J. Zelhofer, Dennis M. Kochmann, On acoustic wave beaming in two-dimensional structural lattices, Int. J. Solids Struct. 115 (2017) 248–269.
[52] David J. Ewins, Modal Testing: Theory, Practice and Application, John Wiley & Sons, 2009.
[53] Martin Isenburg, Stefan Gumhold, Craig Gotsman, Connectivity shapes, in: Proceedings Visualization, VIS'01, IEEE, 2001, pp. 135–552.
[54] Yuanzhen Wang, Beibei Liu, Yiying Tong, Linear surface reconstruction from discrete fundamental forms on triangle meshes, in: Computer Graphics Forum, Vol. 31, No. 8, Wiley Online Library, 2012, pp. 2277–2287.
[55] Davide Boscaini, Davide Eynard, Drosos Kourounis, Michael M. Bronstein, Shape-from-operator: Recovering shapes from intrinsic operators, in: Computer Graphics Forum, Vol. 34, No. 2, Wiley Online Library, 2015, pp. 265–274.
[56] Albert Chern, Felix Knöppel, Ulrich Pinkall, Peter Schröder, Shape from metric, ACM Trans. Graph. 37 (4) (2018) 1–17.
[57] Liao Liu, Mahmoud I. Hussein, Wave motion in periodic flexural beams and characterization of the transition between Bragg scattering and local resonance, J. Appl. Mech. 79 (1) (2012).
[58] Qiaoqiang Gan, Yongkang Gao, Kyle Wagner, Dmitri Vezenov, Yujie J Ding, Filbert J. Bartoli, Experimental verification of the rainbow trapping effect in adiabatic plasmonic gratings, Proc. Natl. Acad. Sci. 108 (13) (2011) 5169–5173.